Temporal and spectral variations of the photoelectron flux and solar irradiance during an X class solar flare.

W.K. Peterson, P.C. Chamberlin, T.N. Woods, and P.G. Richards

Revised 4/27/08

Abstract:

Photoelectrons are the main energy source of airglow used to diagnose the state of the ionosphere-thermosphere system. Because of measurement uncertainties and substantial gaps in the historical record, parameterized models of the EUV irradiance and photoelectron flux are generally used to estimate airglow intensities. This paper compares observed and modeled photoelectron spectra from an X3 class flare that occurred on July 15, 2002.

The photoelectron data were obtained from the FAST satellite. Model photoelectron spectra were obtained from the Field Line Inter-hemispheric Plasma (FLIP) model using 10 s cadence solar spectra at 1 nm resolution from the Flare Irradiance Spectral Model (FISM). The observed and modeled spectra agree well temporally and spectrally within the uncertainties of the models and data. Systematic differences found between observed and modeled photoelectron spectra suggest that the solar irradiance from FISM could be improved at wavelengths shortward of 17 nm.

Introduction:

Photoelectrons play a very important role in the Earth's upper atmosphere. They power the complex thermospheric chemistry and heat the thermal electron and neutral gases. Moreover, photoelectrons are the prime source of airglow that is used to diagnose the state of the ionosphere-thermosphere system. [Richards and Torr, 1985.]

The photoelectron spectrum is produced through photoionization of thermospheric gases by solar EUV irradiance with wavelengths below ~50 nm and so are *in-situ* indicators of solar extreme ultraviolet (EUV) radiation. The incident solar EUV energy is initially split about evenly between ions and photoelectrons. Photoelectron induced airglow has been measured from the ground and used in diagnosing the state of the ionosphere. Similarly, spacecraft measurements of airglow have been used to study the chemistry and dynamics of the ionosphere. In particular, NASA's Atmospheric Explorer and Dynamics Explorer –2 and TIMED satellites have been extensively used to monitor variations in the thermospheric atomic to molecular density ratios [See Strickland et al., 2004, Meier et al., 2005 and references therein]. Furthermore, Strickland et al. [2007] found that the SEE version 8 solar irradiances reported during flares were not consistent with measured airglow and ionospheric electron densities.

Because of measurement uncertainties and substantial measurement gaps in the historical record, several parameterized models of the EUV irradiance and photoelectron flux have been developed [See for example, Lean et al., 2003, Richards et al., 2006, Chamberlin et al., 2007, 2008. and Richards and Peterson, 2008]. As noted by Lean et al., [2003], the differences between these models can only be resolved by comparison with observations. The TIMED satellite has been in orbit taking solar EUV irradiance measurements since February 2002 while the FAST satellite has been making photoelectron measurements since 1997.

The ideal situation for testing the compatibility of Solar EUV irradiance and airglow measurements would be to have simultaneous *in situ* measurements of photoelectron spectra along with the solar irradiance, airglow, and electron density. The ~500 km

perigee of FAST precludes this possibility. However, solar flares provide an opportunity to quantify our understanding of solar energy input to the thermosphere [Woods et al., 2003] using photoelectron observations. This is because photoelectron production is prompt and the variations in both the EUV input and photoelectron response can be examined over a short interval. This eliminates or reduces many of the uncertainties in the observations and models.

In this paper we report measurements from the high altitude FAST satellite of photoelectrons that escape from the upper atmosphere and use them to validate the TIMED/SEE 0-50 nm solar Version 9 EUV irradiance, which has been parameterized for solar flares in the Flare Irradiance Spectral Model (FISM) by Chamberlin et al., [2008] The differences between versons 8 and 9 irradiance data are given by Woods et al. [2008]

Data:

An examination of the FAST data acquired between 1997 and 2006 yielded only one X class flare where appropriate FAST electron data were acquired over the duration of the flare. The top four panels of Figure 1 present spectrograms of photoelectron flux related quantities for the X3 class solar flare that occurred on July 15, 2002. The color legend for each panel is shown to the right of the panel. The GOES-11 solar 0.1-0.8 nm X-ray flux is shown in Panel 5 of Figure 1. According to the NOAA flare database (http://www.ngdc.noaa.gov/stp/SOLAR/ftpsolarflares.html#xray) the flare began at 19:59, reached it maximum at 20:08, and ended at 20:14. During this interval the FAST satellite [Pfaff et al., 2001] was at an altitude of ~3700 km equatorward of the auroral oval near the terminator. The electron spectrometer on FAST [Carlson et al., 2001] was

turned on at 20:01 UT, just a minute after flare onset and continued to measure photoelectrons until it entered the auroral oval at 20:15. After 20:15 the electron signal was not useable because of auroral electrons.

Panel 6 of Figure 1 shows that the solar zenith angle in the ionosphere decreased from 95 to 85 degrees. The measurements of Lee et al. [1980] and models indicate that at high altitudes the upward photoelectron flux varies little with solar zenith angle until it exceeds 95 degrees. Thus, the topside of the ionosphere was fully illuminated by solar ultraviolet radiation throughout the measurement interval. Models also show that, except at the well-known peaks between 20 and 30 eV, the ionospheric photoelectron flux is not sensitive to neutral composition [Richards and Torr, 1985]. In any case, the escape flux comes from high altitudes where O is the dominant neutral species. In addition, for energies below ~20 eV, the photoelectron flux becomes increasingly influenced by Coulomb collisions with the topside ionosphere thermal electron population. For this reason, we do not report fluxes below 15 eV in Figure 1. As a result of its insensitivity to solar zenith angle and neutral density, the greater than 20 eV escape flux that reaches the FAST satellite accurately monitors changes in solar EUV irradiance [See discussion by Richards and Peterson, 2008].

Panel 1 of Figure 1 presents an energy-time spectrogram of 10s averages of the flux of electrons detected as a function of time. The observed photoelectron spectra have been adjusted to account for the spacecraft potential and a background signal caused by penetrating radiation has been removed as described by Woods et al. [2003]. The photoelectron intensity in units of electrons/cm^2-s-sr-eV is encoded using the color bar on the right. Panel 2 of Figure 1 shows the relative changes in photoelectron flux as a

function of time for each energy bin where relative change is defined as the difference between the observed flux and the average flux in each energy bin divided by the average flux in each energy bin.

Figure 2 shows line plots of 10s averages of the photoelectron flux as a function of time for six selected energies. The line plots show that the high energy Auger electrons at 364 and 536 eV increase sharply around 2 minutes while the other energies do not increase significantly until more than 3 minutes have elapsed. This supports the conclusion that cascade from higher energies is not a significant contributor to the 4 lower energy fluxes. If cascade were important, the 101 eV flux would be expected to rise in concert with the higher energy fluxes. The effects of cascade from higher energies however are expected be significantly greater in the collisional environment at ~ 110 km where most of the energy from the high energy Auger electrons is deposited. The behavior of the 3 fluxes below 60 eV differs from the 3 higher energy fluxes in that they remain steady between 5 and 11 minutes while the higher energy fluxes continue to increase and then decrease. It is also interesting to note that the 25.5 and 31.4 eV fluxes increase slightly more between 3 and 5 minutes than do the 55.9 and 101 eV fluxes.

As noted by Woods et al., [2003] the absolute uncertainty of the photoelectron fluxes shown is about 40%. However, because the electron optics of the detector are well defined, the uncertainty in the energy spectral shape and temporal evolution is significantly less. Table 1 presents the relative one-sigma uncertainty in the flux values (i.e. 68% confidence levels) based on the number of signal counts for the energy/time bins at 20:03, 20:08, and 20:13. Table 1 also shows the wavelength limits in nm corresponding to the solar EUV photons that contribute photoelectrons in that energy

range accepted by the FAST electron detector between the 50% response energies, the so called full width at half maximum (FWHM). The principal solar EUV features related to each energy range are also noted. The wavelength ranges have been obtained by noting that photoionization of atomic oxygen is the principal source of the escaping photoelectrons for most of the energy range; Auger ionization of N_2 being a major exception. We note here that during non-flare times the photoelectron intensity falls off rapidly at energies above 60eV. This is referred to as the 60 eV knee in the spectrum [Doering et al., 1975, Peterson et al., 1977].

There were no solar irradiance observations from either the TIMED [Woods et al., 2005] or RHESSI [Lin et al., 2002] satellites during this flare so we used the Flare Irradiance Spectral Model (FISM) [Chamberlin et al., 2008]. The FISM model is based on 39 selected solar flare observations made by the TIMED/SEE instrument and the GOES X-ray sensor [Garcia, 1994]. Panel 3 of Figure 1 shows the relative change of the FISM model 0-50 nm solar irradiance at a 10s cadence using the same algorithm that was used for photoelectrons in panel 2. Because shorter wavelengths correspond to larger photoelectron energies, it is difficult to compare the relative changes in FAST photoelectron flux and solar irradiance directly. However, the short wavelength bright region between 20:05 and 20:10 in panel 3 corresponds to the high energy bright region in panel 2.

A more informative comparison of the observed photoelectron flux and solar irradiance requires an ionosphere-plasmasphere model that takes into account the relevant processes. We use the Field Line Inter-hemispheric Plasma (FLIP) model, which calculates the plasma densities and temperatures and includes a 2-stream model of the

photoelectron flux [Richards et al. 2006; Richards and Peterson, 2008]. For these calculations, the non-flare HEUVAC EUV irradiance model [Richards et al., 2006] has been replaced by irradiance predictions from the FISM model at 10s cadence and 1nm resolution. Panel 4 of Figure 1 shows the ratio (PE_meas-PE_model)/PE_model as a function of energy in energy-time spectrogram format. Overall, the agreement is very good with the biggest difference being between ~80 and ~150 eV (~13-8 nm) where the model flux underestimates the measured flux substantially. Figure 3 shows line plots of this ratio at the selected energies shown in Table 1.

The major differences between the modeled and observed photoelectron fluxes occur during the impulsive phase of the flare before 20:05 [Schrijver and Zwaan, 2000]. In Figure 1, except near the peak of the flare, the observations are consistently larger than those obtained from the FLIP model driven by dynamic FISM solar EUV spectra. Other notable features in Figure 1 include higher than modeled photoelectron fluxes in the 20-35 eV range between 20:03 and 20:05 and generally lower than modeled photoelectron fluxes above ~150 eV from ~20:05 to ~20:10.

Discussion

The photoelectron data presented here are the first to document temporal variations in photoelectron spectral intensity over an interval including most of an X class flare. The agreement in the temporal evolution of the photoelectron spectral shape and that predicted using the FLIP and FISM models shown in Figures 1 and 3 is remarkably good. At energies below the 60 eV knee in the photoelectron spectra the relative differences between the observed and modeled fluxes are less than 50% for the entire interval. The

1 best agreement between observed and modeled photoelectron fluxes occurs after 20:05
2 during the gradual phase of the flare [Schrijver and Zwaan, 2000] at energies below the
3 60 eV knee. The differences in this limited temporal and spectral domain are quite
4 remarkable. They are less than 30%.

5 The FISM flare results are based on data obtained by the TIMED/SEE instrument
6 during 39 selected flares [Chamberlin et al., 2008]. Below 27 nm TIMED/SEE data are
7 obtained from broadband (~5-10 nm) detectors. These broadband data are divided into 1
8 nm bins using high resolution reference spectra as described in Woods et al., [2005].
9 Chamberlin et al., [2008] estimates that below 30 nm the uncertainty of the FISM model
10 during the gradual phase of a flare is wavelength dependent and ranges from 40% to over
11 100%. These differences are within the relative differences shown in Figures 1 and 3 in
12 the uncertainties of the models in this temporal (after 20:05) and spectral (above 25 eV)
13 range. Nevertheless the systematic differences reported in Panel 4 of Figure 1 suggest
14 improvements that could be made to FISM.

15 Some of the differences shown in Panel 4 are likely due to systematically low values
16 in the FISM irradiances at shorter than 10 nm during non-flare times. In contrast, the
17 daily averaged photoelectron flux predictions from FLIP using the HEUVAC model
18 results, instead of FISM, indicate good agreement with the FAST measured photoelectron
19 fluxes above the 60 eV knee for times before 20:05 [Woods et al., 2008]. The FISM
20 results at shorter than 27 nm are based on the TIMED and SORCE XPS results that
21 include fitting higher resolution solar spectral models to the broadband (7-10 nm) XPS
22 measurements. The spectral differences near 10 nm between HEUVAC and FISM (and
23 inferred from differences in the photoelectron flux near 100 eV) are probably related to

differences in original calibration uncertainties for the solar XUV measurements, nature of using broadband XPS measurements to scale higher resolution model spectra, and uncertainties in the spectral distribution within the model spectra. These differences in the photoelectron fluxes before 20:05 can also be related to how well FISM describes the solar irradiance during the impulsive phase of the flare.

The systematic differences between photoelectron data and model data presented here suggest that the FISM model could be improved in the spectral range below 27 nm, especially near 10 nm and for non-flare times and during the impulsive phase of the flare. As noted by Chamberlin et al., [2008] the limitations of the FISM model below 27 nm arise because of the small number of large solar flares (39) used to construct the model and uncertainties arising from portioning energy from the broadband (5-10 nm) detectors to the 1 nm resolution required for aeronomic investigations. Improvement of the FISM model will require analysis of existing data and data from new instruments. Photoelectron observations are available from the FAST satellite during most of the last solar cycle (i.e. since January, 1997). Comparison of these observations with modeled photoelectron data driven by a variety of model solar EUV spectra will show if the systematic differences noted here above the 60 eV photoelectron knee exist during non flare times. There are only a small number of impulsive phase measurements used in developing FISM, so further progress in understanding spectral changes during the impulsive phase is pending on new observations during flares of either the photoelectrons or higher spectral resolution solar EUV spectra, as planned with the SDO EUV Variability Experiment (EVE) at 0.1 nm resolution and with 10-sec cadence [Woods et al., 2006]. The results presented here can be used to validate other flare irradiance models such as the one

proposed by Rodgers et al. [2006] if a suitable overlap between TIMED/SEE and FAST operations can be found in the next solar cycle.

Acknowledgements:

This research was supported by NASA grants NNG05GK153 and NNX07AB68G to the University of Colorado and NASA grant NNX07AN03G to George Mason University.

References

Carlson, C.W., J.P. McFadden, et al., (2001), The electron and ion plasma experiment for FAST, Space Sci. Rev. 98, 33.

Chamberlin, P. C., T. N. Woods, and F. G. Eparvier (2007), Flare Irradiance Spectral Model (FISM): Daily component algorithms and results, Space Weather, 5, S07005, doi:10.1029/2007SW000316.

Chamberlin, P. C., T. N. Woods, and F. G. Eparvier (2008), Flare Irradiance Spectral Model (FISM): Flare component algorithms and results, *Space Weather*, In Press, doi:10.1029/2007SW000372.

Doering, J.P., W.K. Peterson, C.O. Bostrom and J.C. Armstrong (1975), Measurement of low-energy electrons in the day airglow and day side auroral zone from Atmosphere Explorer C, *J. Geophys. Res. 80*, 3934.

Garcia, H. (1994), Temperature and emission measure from GOES soft X-ray measurements, *Solar Phys., 154*, 275.

Lean, J.L., H.P. Warren, J.T. Mariska, and J. Bishop (2003), A new model of solar EUV irradiance variability: 2. Comparisons with empirical models and observations and

implications for space weather. J. Geophys. Res. 108 (A2), 1059, doi:10.1029/2001JA009238.

Lee, J. S., J. P. Doering, T. A. Potemra, and L. H. Brace, (1980), Measurements of the Ambient photoelectron spectrum from Atmosphere Explorer: II. AE-E measurements from 300 to 1000 km during solar minimum conditions, *Planet. Space Sci.*, 28, 973-996.

Lin, R.P., et al., (2002), The Reuven Ramaty High-Energy Solar Spectroscopic Imager (RHESSI), Solar Physics, 210, 3, doi:10.1023/A:1022428818870.

Meier, R., G. Crowley, D. J. Strickland, A. B. Christensen, L. J. Paxton, D. Morrison, and C. L. Hackert (2005), First look at the 20 November 2003 superstorm with TIMED/GUVI: Comparisons with a thermospheric global circulation model, J. Geophys. Res., 110, A09S41, doi:10.1029/2004JA010990.

Peterson, W.K. et al. (1977), Measurement of magnetic field aligned potential differences using high resolution conjugate photoelectron energy spectra, *Geophys. Res. Lett* 4, 373.

Pfaff, R., C. Carlson, J. Watzin, D. Everett, and T. Gruner, (2001), An overview of the FAST auroral Snapshot (FAST) satellite, *Space Sci. Rev*., 98, 1.

Richards, P.G., and Torr, D.G., (1985), The altitude variation of the ionospheric photoelectron flux: a comparison of theory and measurement," *J. Geophys. Res*., 90, 2877-2884.

Richards, P.G., T. N. Woods, and W. K. Peterson, (2006), HEUVAC: A new high resolution Solar EUV proxy model, *Adv. Space Res*., *37*, 315-322.

Richards, P. G. and W. K. Peterson, (2008), Experimental validation of theoretical photoelectron fluxes in the plasmasphere, *Submitted to JGR, February 2008*.

Rodgers, E. M., S. M. Bailey, H. P. Warren, T. N. Woods, and F. G. Eparvier (2006), Soft X-ray irradiances during solar flares observed by TIMED-SEE, J. Geophys. Res., 111, A10S13, doi:10.1029/2005JA011505.

Strickland, D. J., R. R. Meier, R. L. Walterscheid, J. D. Craven, A. B. Christensen, L. J. Paxton, D. Morrison, and G. Crowley (2004), Quiet-time seasonal behavior of the thermosphere seen in the far ultraviolet dayglow, *J. Geophys. Res*., *109*, A01302, doi:10.1029/2003JA010220.

Strickland, D. J., et al. (2007), Constraining and validating the Oct/Nov 2003 X-class EUV flare enhancements with observations of FUV dayglow and E-region electron densities, J. Geophys. Res., 112, A06313, doi:10.1029/2006JA012074.

Schrijver, C.J. and C. Zwaan (2000), *Solar and stellar magnetic activity*, Cambridge University Press, Cambridge.

Woods, T.N., S.M. Bailey, W.K. Peterson, S.C. Solomon, H.P. Warren, F.G. Eparvier, H. Garcia, C.W. Carlson, and J.P. McFadden, (2003), Solar Extreme Ultraviolet Variability of the X-Class Flare on April 21, 2002 and the Terrestrial Photoelectron Response, Space Weather, 1, 1001, doi:10.1029/2003SW000010.

Woods, T.N., F.G. Eparvier, S.M. Bailey, P.C. Chamberlin, J. lean, G.J. Rottman, S.C. Solomon, W.K. Tobiska, D.L. Woodraska, (2005), The Solar EUV Experiment (SEE): Overview and prime mission results, *J. Geophys. Res*., 110, A01312, doi: 10.1029/2004JA010765.

Woods, T. N., J. L. Lean, and F. G. Eparvier (2006), The EUV variability experiment (EVE): Science plans and instrument overview, *International Living With a Star (ILWS) Proceedings*, Goa, India, edited by N. Gopalswamy and A. Bhattacharyya, ISBN 81-87099-40-2, p. 145.

Woods, T.N. et al., (2008), XUV Photometer System (XPS): Improved solar irradiance algorithm using Chianti spectral models, Submitted to Solar Physics, 2008.

Table1

PE Energy (eV)	Flux Uncertainty at 20:03 (%)	Flux Uncertainty at 20:08 (%)	Flux Uncertainty at 20:13 (%)	Solar wavelengths at FWHM of electron detector (nm)		Solar Features
25.5	2	1	1	26.7	32.5	He, Si
31.4	2	2	2	23.7	28.4	Fe, He, S, Si
55.9	5	4	4	15.7	18.8	Fe
101.0	12	8	8	9.7	11.6	Fe et al.
363.6	21	14	10	3.1	3.5	N_2 Auger
536.1	22	16	14	2.1	2.4	Ox Auger

Table 1. Relative one-sigma uncertainty derived from instrumental count rates in the flux values for selected energies and times. Wavelength limits in nm corresponding the energy range accepted. See text.

Figures

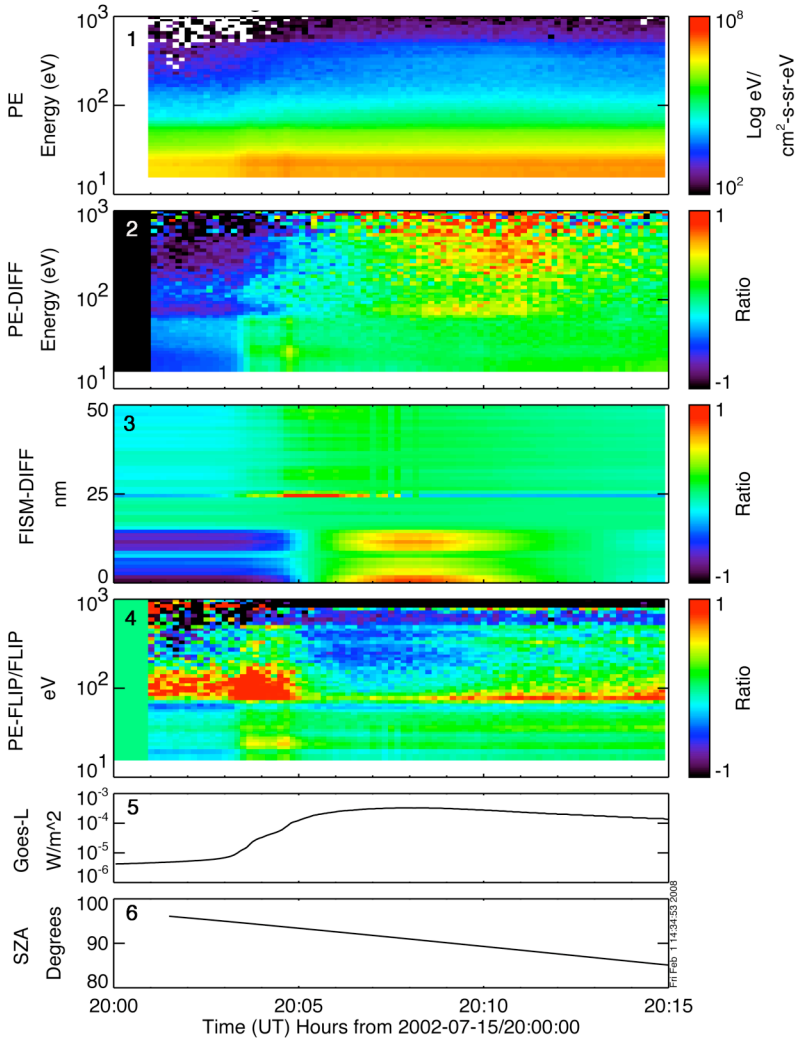

Figure 1: Data acquired during the X3 class solar flare on July 15, 2002. Top panel: Observed photoelectron flux intensity as a function of energy in units of electrons/cm2-s-sr-eV encoded using the color bar on the right. Second panel: Relative changes of the photoelectron flux. Third Panel: Relative changes in the input EUV solar spectra. Fourth Panel: Relative differences between observed and modeled photoelectron fluxes. Fifth panel: Intensity of the Solar X-ray flux in the 0.1 to 0.8 nm range. Bottom panel: Solar zenith angle at the foot of a magnetic field line passing through the FAST satellite.

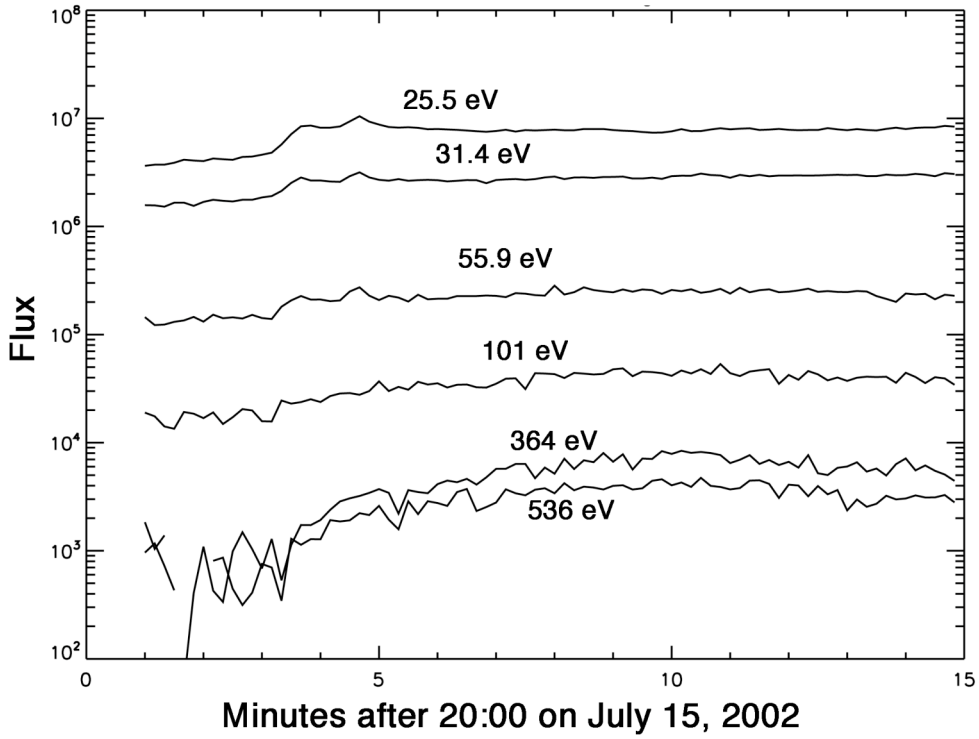

Figure 2: Photoelectron flux intensity in units of (cm-s-sr-eV)$^{-1}$ as a function of time for selected energies shown in Figure 1. See Table 1 for the observational uncertainties at selected times.

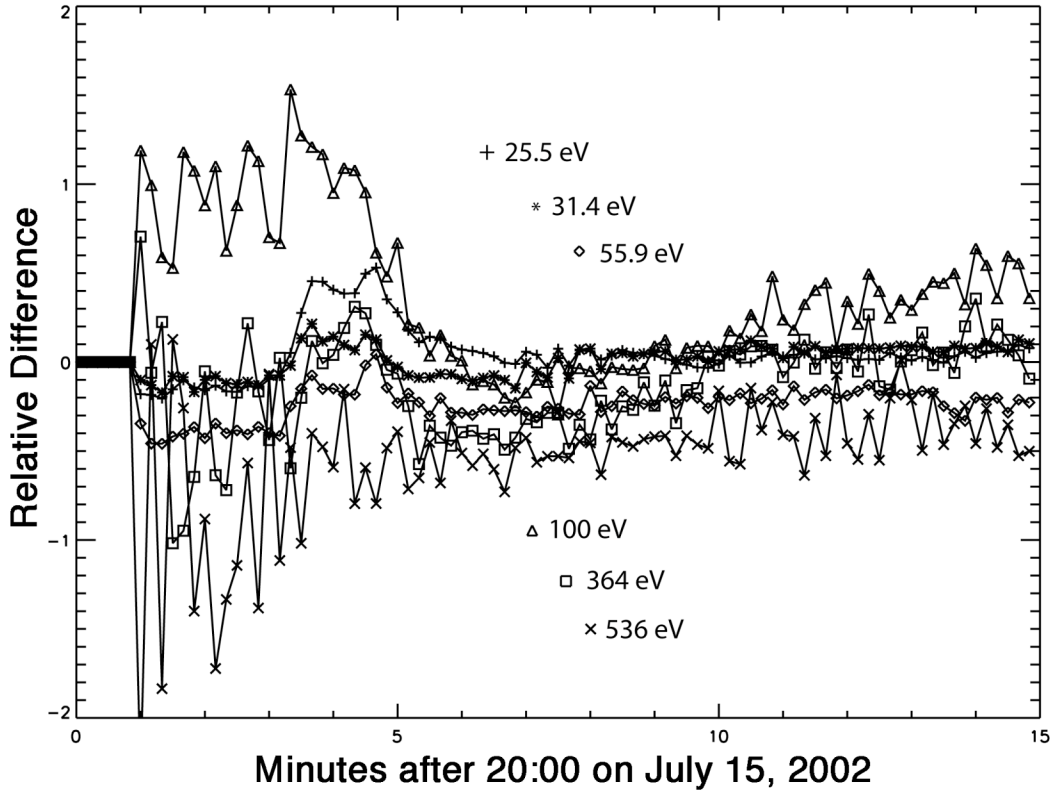

Figure 3: Relative differences between observed and modeled photoelectron fluxes at selected energies. See text.